Journal of Biomechanics 45 (2012) 2698–2701

Contents lists available at SciVerse ScienceDirect

Journal of Biomechanics

journal homepage: www.elsevier.com/locate/jbiomech
www.JBiomech.com

Short communication

Beyond finite elements: A comprehensive, patient-specific neurosurgical simulation utilizing a meshless method

K. Miller *, A. Horton, G.R. Joldes, A. Wittek

Intelligent Systems for Medicine Laboratory, The University of Western Australia, Crawley, Perth, Western Australia 6909, Australia

ARTICLE INFO

Article history:
Accepted 27 July 2012

Keywords:
Neurosurgical simulations
Patient-specific simulations
Registration
Meshless methods
Total Lagrangian Formulation

ABSTRACT

To be useful in clinical (surgical) simulations, a method must use fully nonlinear (both geometric and material) formulations to deal with large (finite) deformations of tissues. The method must produce meaningful results in a short time on consumer hardware and not require significant manual work while discretizing the problem domain. In this paper, we showcase the Meshless Total Lagrangian Explicit Dynamics Method (MTLED) which meets these requirements, and use it for computing brain deformations during surgery. The problem geometry is based on patient-specific MRI data and includes the parenchyma, tumor, ventricles and skull. Nodes are distributed automatically through the domain rendering the normally difficult problem of creating a patient-specific computational grid a trivial exercise. Integration is performed over a simple, regular background grid which does not need to conform to the geometry boundaries. Appropriate nonlinear material formulation is used. Loading is performed by displacing the parenchyma surface nodes near the craniotomy and a finite frictionless sliding contact is enforced between the skull (rigid) and parenchyma. The meshless simulation results are compared to both intraoperative MRIs and Finite Element Analysis results for multiple 2D sections. We also calculate Hausdorff distances between the computed deformed surfaces of the ventricles and those observed intraoperatively. The difference between previously validated Finite Element results and the meshless results presented here is less than 0.2 mm. The results are within the limits of neurosurgical and imaging equipment accuracy (~1 mm) and demonstrate the method's ability to fulfill all of the important requirements for surgical simulation.

1. Introduction

In their influential review Nakaji and Spetzler (2004) list the "accurate localization of the target" as the first principle in modern surgical approaches. As only the preoperative anatomy of the patient is known precisely from medical images, it is now recognized that the ability to predict soft organ deformation (and therefore intraoperative anatomy) during the operation is the main problem in performing reliable surgery on soft organs. Our aim is to simulate the deformation of the entire brain using information from preoperative MRIs and the knowledge of the position of the portion of the brain surface exposed by craniotomy. The simulation we present is based on MRI data which has already been used for FEM simulation and model validation in Wittek et al. (2010). The surgical procedure involved removing a section of the skull immediately over the large anterior tumor, after which a significant retraction of the cortical surface was observed near the craniotomy.

Calculations of soft tissue deformation have historically been built on Finite Element Analysis (Cotin et al., 1999; Ferrant et al., 2001; Luboz et al., 2005; Picinbono et al., 2003) with promising results. In Wittek et al. (2010) we demonstrated that a high level of precision can be achieved in patient-specific simulations of surgical procedures using non-linear (both geometric and material) biomechanical models. The accuracy of the Finite Element calculations depends heavily on the mesh which discretizes the geometry, so it is desirable to use only good quality hexahedral elements (Yang and King, 2011). With highly irregular geometry, an experienced analyst is required to create a patient-specific mesh, which consumes valuable human time. From our experience (Wittek et al., 2010) tedious manual mesh correction is still necessary even with recently developed software for generation of anatomic Finite Element meshes such as IA-FEMesh by Grosland et al. (2009).

One solution to this challenge is to use a numerical method that does not require so strict a spatial discretization, such as a meshless method. Various meshless (or Element-Free) methods have been presented as alternatives to Finite Element methods (Babuska and Melenk, 1997; Belytschko et al., 1994; Li and Liu, 2004; Liu, 2003; Melenk and Babuška, 1996). These have primarily

* Corresponding author.
E-mail address: kmiller@mech.uwa.edu.au (K. Miller).

0021-9290/$ - see front matter © 2012 Elsevier Ltd. All rights reserved.
http://dx.doi.org/10.1016/j.jbiomech.2012.07.031

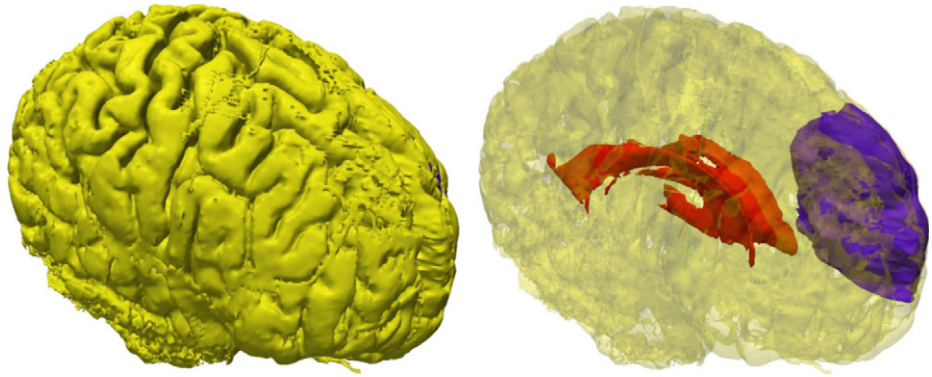

Fig. 1. Surface visualizations of the problem geometry; Parenchyma (yellow), Tumor (blue) and Ventricle (Red). (For interpretation of the references to color in this figure legend, the reader is referred to the web version of this article.)

been motivated by the study of fracture mechanics and large deformations. Efforts to apply these methods in surgical simulation have been very limited (Doblare et al., 2005; Horton et al., 2007) and, to date, inadequate for clinical use.

In this paper, we showcase a suit of meshless algorithms which can deal with irregular 3D geometries composed from multiple parts, large deformations, non-linear, almost incompressible materials and contacts. It allows automatic discretization of the problem domain and is sufficiently fast to produce clinically useful results in a short time using only easily-available consumer hardware.

2. Methods

2.1. Problem geometry

This is a real-world, patient-specific 3D geometry with all the irregularities that can be expected in clinical simulations. Fig. 1 shows the anatomical components as surfaces generated from the segmented MRIs. The parenchyma, tumor and ventricle volumes were filled with a total of 31,753 nodes with average spacing of 3.5 mm. Discretizing the irregular geometry in this way is a trivial exercise, whereas creating a good quality Finite Element mesh for the same geometry was a tedious and time-consuming, semi-automatic effort requiring a lot of manual intervention. The rigid skull was represented by its internal surface (Fig. 2).

2.2. Background integration grid

One way to integrate across the volume is to use a background mesh, but this requires manual work and largely defeats the purpose of using a meshless method. For this simulation, a regular Cartesian grid of 53,672 integration points was created within the problem domain with 3 mm spacing between points. Such a grid can contain a small volume error (at most half of a volume of a hexahedron intersected by a domain boundary) because the grid is not volume-conforming but this has proven to be too small to have any significant effect on the results in all simulations to date (Horton et al., 2010, 2007). The freedom and simplicity offered by such a background grid outweigh the small inaccuracy.

2.3. Boundary conditions and loading

We defined a contact interface between the skull and the parenchyma surface. Nodes on the parenchyma surface could not penetrate the skull, but could slide without friction as in Wittek et al. (2010). The tumor and ventricle surfaces were tied (by shared nodes) to the internal surfaces of the parenchyma.

To load the model, we prescribed displacements on the portion of the parenchyma surface which had been exposed by the craniotomy (see Fig. 2). The displacement for each loaded node was determined from distances between the preoperative and intraoperative parenchyma surfaces in the segmented MRIs.

2.4. Material Properties

Following Wittek et al. (2009, 2010) we used Neo-Hookean constitutive model with parameters given in Table 1. From solid-mechanical perspective our simulation belongs to the special class called displacement-zero traction problems whose solution is known to be weakly dependent on the unknown patient-specific properties of tissues (Ciarlet, 1988; Neal and Kerckhoffs, 2010; Wittek et al., 2009).

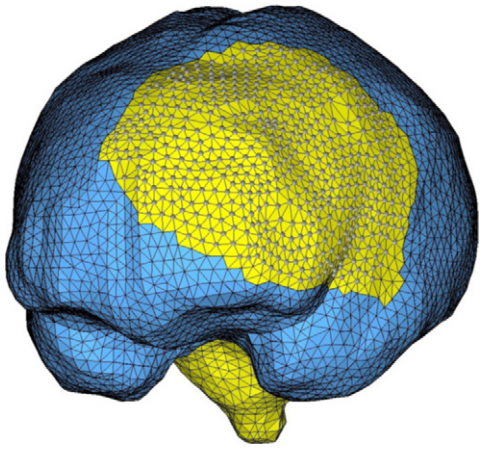

Fig. 2. Triangulated skull surface (blue). The parenchyma surface (yellow) is visible through the craniotomy. Part of the brain stem (yellow) is also visible where it protrudes from the base of the skull. Also shown are the loaded nodes on the surface of the parenchyma exposed by the craniotomy. (For interpretation of the references to color in this figure legend, the reader is referred to the web version of this article.)

Table 1
Material properties for each component in the simulation. μ and λ are the Lamé parameters.

Parameter	Parenchyma	Tumor	Ventricles
μ (Pa)	1.007×10^3	2.013×10^3	4.56
λ (Pa)	49.33×10^3	98.66×10^3	1.14
Poisson's ratio	0.49	0.49	0.1
Mass density (kg m^{-3})	10^3	10^3	10^3

Following Wittek et al. (2007), the skull was modeled as rigid since its stiffness is several orders of magnitude greater than that of all the other simulated parts.

2.5. Suite of algorithms

2.5.1. Solution algorithm

We used Meshless Total Lagrangian Explicit Dynamics solution algorithm. Horton et al. (2010) describe and verify the algorithm as well as provide recommendations about node placement and relative ratio of nodes to integration points.

2.5.2. Time-step selection

In this simulation we used constant time step estimated based on the linearized theory (Joldes et al., 2012).

2.5.3. Termination criterion

To terminate the simulation we used a displacement error estimation as described in (Joldes et al., 2009a).

2.5.4. Contact algorithm

We used frictionless finite sliding contact as described in Joldes et al. (2008).

2.5.5. Determination of correspondence between pre- and intraoperative brain surfaces

This correspondence was determined by applying a vector-spline regularization algorithm (Arganda-Carreras et al., 2006) to the surface curvature maps (Joldes et al., 2009b).

3. Results

3.1. Cross sections

We show six 2D sections, taken at 5 mm intervals, through regions of the brain which involve all the major anatomical components (Fig. 3). We also compare our results to those obtained with a high quality FE mesh which was presented and validated in Wittek et al. (2010).

3.2. Hausdorff distances

Following Archip et al. (2007), Oguro et al. (2011), Wittek et al. (2010), we used the 95% Hausdorff distance to objectively measure the differences between the intraoperative surfaces of the major anatomical structures of the brain predicted using the MTLED-based method and the surfaces obtained through segmentation of the intraoperative MRIs, Fig. 4.

3.3. Computational efficiency

The simulation presented here was performed on a machine with an Intel Core i7 930 2.8 GHz processor and 4 GB of physical memory. The calculation time of our fully nonlinear problem with almost 100,000 degrees of freedom was 19.2 s for the approximately 1000 time steps required to obtain convergence. Such an excellent computational efficiency is due to the fully explicit nature of our algorithm and the use of Total Lagrangian Formulation.

4. Discussion and conclusions

We used MTLED-based suite of algorithms to perform a comprehensive patient-specific surgical simulation. The contours in Fig. 3 show good similarity between the MTLED and FE results. Only in a few places are slightly different results seen and the differences are not larger than the voxel size of the intraoperative brain MRI (which is of an order of $0.86 \times 0.86 \times 2.5\ \mathrm{mm}^3$). From this comparison, it appears that from the perspective of

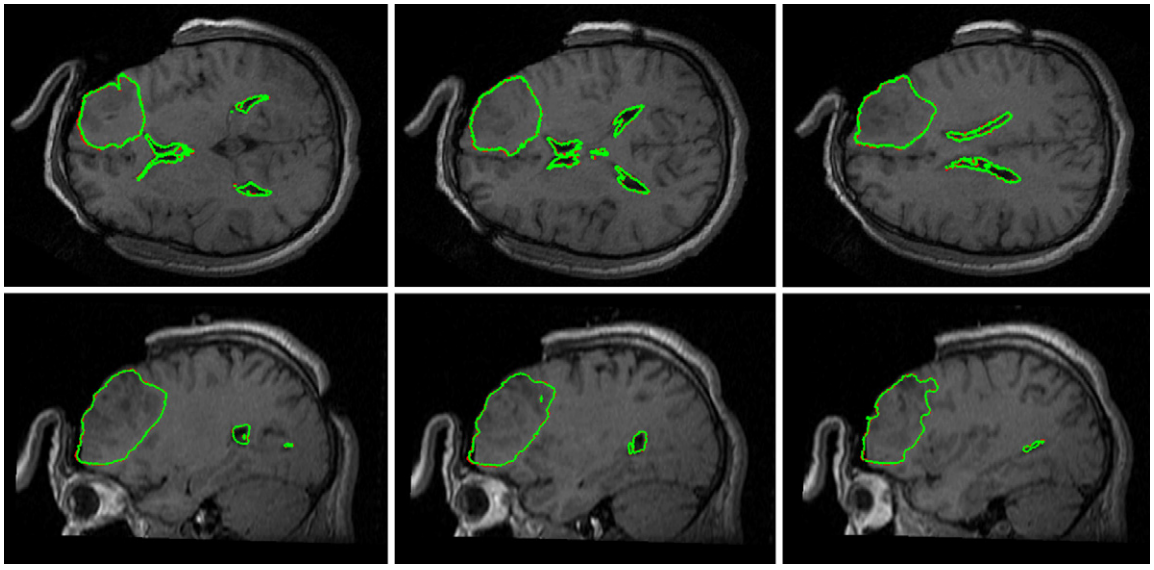

Fig. 3. Intraoperative MRIs overlaid with contours (green lines) of the deformed tumor and ventricle surfaces as generated by our MTLED-based suite of algorithms. The three transverse sections (top row) and three sagittal sections (bottom row) were taken at 5 mm intervals. For reference, the red lines represent the contours of the deformed ventricles and tumor computed by FEM, but these are almost entirely obscured by the very similar MTLED results. (For interpretation of the references to color in this figure legend, the reader is referred to the web version of this article.)

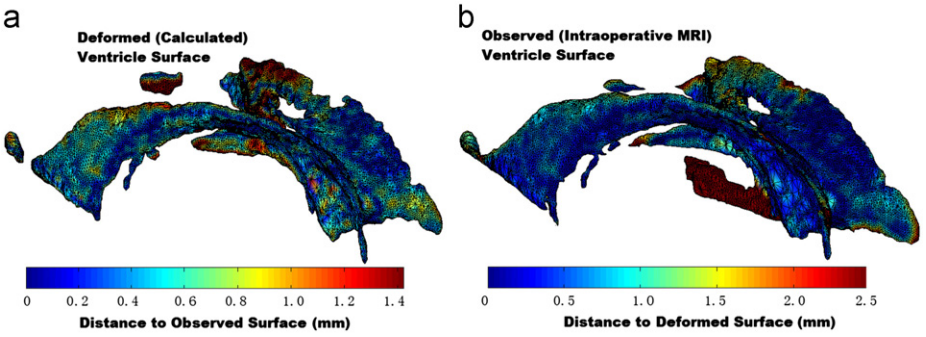

Fig. 4. Differences between calculated (Surface A) and intraoperatively observed (Surface B) ventricle surfaces. The left image shows the calculated ventricle surface A (based on the segmented preoperative MRIs and deformed by the MTLED algorithm). The colors represent the distance $d(a,B)$ from point a on Surface A to the nearest point on Surface B generated from the segmented intraoperative MRIs. The scale reaches 95% Hausdorff Distance $H_{95}(A,B)$. Similarly, the right image shows the surface B, with colors representing the distance $d(b,A)$. (For interpretation of the references to color in this figure legend, the reader is referred to the web version of this article.)

image-guided surgery, the results obtained using the MTLED method are as useful and accurate as those obtained with the FE method. Considering the reduced complexity of model generation, this is an excellent result and makes algorithms of this sort a viable option for clinical use.

Looking at the color codes in Fig. 4, we see that the majority of the surfaces (blue) agree to within 1 mm. Since this is the level of accuracy in image guided surgery (Bourgeois et al., 1999; Warfield et al., 2005), we can make the claim that the results are accurate enough to be useful in clinical situations. Note however the localized region of high discrepancy in the right-hand side image in Fig. 4 and the resulting larger value for h_{95}(B, A). This is a consequence of the entire third ventricle in the segmented intraoperative MRI that was not present in the segmented preoperative MRIs. Comparison of the two images in Fig. 4 and good agreement of the predicted intraoperative contours of the tumor and ventricles with the intraoperative images (Fig. 3) suggest that the localized region of discrepancy in the right-hand side image in Fig. 4 is due to the differences in ventricle segmentations of the preoperative and intraoperative images rather than inaccuracies in predicting the intraoperative deformations.

We simulated a craniotomy-induced brain shift with over 30,000 nodes and 50,000 integration cells and obtained results within half a minute. This is certainly fast enough to be used in clinical situations. However, there is excellent scope to increase the speed of this algorithm by employing GPUs to handle the very parallel calculations (Joldes et al., 2010). Therefore clinically useful results can be obtained without the need for supercomputers.

Conflict of interest statement

The authors have no conflicts of interest in this study.

Acknowledgments

This work was supported by ARC Grants DP1092893 and DP120100402 and NHMRC Grant APP1006031. Segmented pre- and intraoperative MRI data were provided by the Computational Radiology Laboratory, Harvard with funding in part from NIH Grants R01 EB008015 and R01 LM010033, and by a Research Grant from the Children's Hospital Boston Translational Research Program.

References

Archip, N., Clatz, O., Whalen, S., Kacher, D., Fedorov, A., Kot, A., Chrisochoides, N., Jolesz, F., Golby, A., Black, P.M., Warfield, S.K., 2007. Non-rigid alignment of pre-operative MRI, fMRI, and DT-MRI with intra-operative MRI for enhanced visualization and navigation in image-guided neurosurgery. NeuroImage 35, 609–624.

Arganda-Carreras, I., Sorzano, C.O.S., Marabini, R., Carazo, J.M., Ortiz-de-Solorzano, C., Kybic, J., 2006. Consistent and elastic registration of histological sections using vector-spline regularization. Computer Vision Approaches to Medical Image Analysis 4241, 85–95.

Babuska, I., Melenk, J.M., 1997. The partition of unity method. International Journal for Numerical Methods in Engineering 40, 727–758.

Belytschko, T., Lu, Y.Y., Gu, L., 1994. Element-free Galerkin methods. International Journal for Numerical Methods in Engineering 37, 229–256.

Bourgeois, G., Magnin, M., Morel, A., Sartoretti, S., Huisman, T., Tuncdogan, E., Meier, D., Jeanmonod, D., 1999. Accuracy of MRI-guided stereotactic thalamic functional neurosurgery. Neuroradiology 41, 636–645.

Ciarlet, P.G., 1988. Mathematical elasticity, Three-dimensional Elasticity. North Holland, The Netherlands.

Cotin, S., Delingette, H., Ayache, N., 1999. Real-time elastic deformations of soft tissues for surgery simulation. IEEE Transactions on Visualization and Computer Graphics 5, 62–73.

Doblare, M., Cueto, E., Calvo, B., Martinez, M., Garcia, J., Cegonino, J., 2005. On the employ of meshless methods in biomechanics. Computer Methods in Applied Mechanics and Engineering 194, 801–821.

Ferrant, M., Nabavi, A., Macq, B., Jolesz, F.A., Kikinis, R., Warfield, S.K., 2001. Registration of 3-D intraoperative MR images of the brain using a finite-element biomechanical model. IEEE Transactions on Medical Imaging 20, 1384–1397.

Grosland, N.M., Shivanna, K.H., Magnotta, V.A., Kallemeyn, N.A., DeVries, N.A., Tadepalli, S.C., Lisle, C., 2009. IA-FEMesh: An open-source, interactive, multi-block approach to anatomic finite element model development. Computer methods and programs in biomedicine 94, 96–107.

Horton, A., Wittek, A., Joldes, G.R., Miller, K., 2010. A meshless Total Lagrangian explicit dynamics algorithm for surgical simulation. International Journal for Numerical Methods in Biomedical Engineering 26, 977–998.

Horton, A., Wittek, A., Miller, K., 2007. Subject-specific biomechanical simulation of brain indentation using a meshless method. In: Ayache, N., Ourselin, S., Maeder, A. (Eds.), Proceedings of the10th International Conference on Medical Image Computing and Computer-Assisted Intervention. vol. 4791, Brisbane, Australia Published in Lecture Notes in Computer Science, pp. 541–548.

Joldes, G.R., Wittek, A., Miller, K., 2009a. Computation of intra-operative brain shift using dynamic relaxation. Computer Methods in Applied Mechanics and Engineering 198, 3313–3320.

Joldes, G.R., Wittek, A., Miller, K., 2009b. Cortical surface motion estimation for brain shift prediction. In: Miller, K., Nielsen, P.M.F. (Eds.), Computational Biomechanics for Medicine IV Workshop. MICCAI, London, UK, pp. 50–59.

Joldes, G.R., Wittek, A., Miller, K., 2010. Real-time nonlinear finite element computations on GPU-application to neurosurgical simulation. Computer Methods in Applied Mechanics and Engineering 199, 3305–3314.

Joldes, G.R., Wittek, A., Miller, K., 2012. Stable time step estimates for mesh-free particle methods. International Journal for Numerical Methods in Engineering 9(4), 450–456 , http://dx.doi.org/10.1002/nme.4290.

Joldes, G.R., Wittek, A., Miller, K., Morriss, L., 2008. Realistic and efficient brain-skull interaction model for brain shift computation. In: Miller, K., Nielsen, P.M.F. (Eds.), Computational Biomechanics for Medicine III Workshop. MICCAI, New-York, pp. 95–105.

Li, S., Liu, W.K., 2004. Meshfree Particle Methods. Springer Verlag, Berlin.

Liu, G.R., 2003. Mesh free Methods: Moving Beyond the Finite Element Method. CRC Press, Boca Raton, FL.

Luboz, V., Chabanas, M., Swider, P., Payan, Y., 2005. Orbital and maxillofacial computer aided surgery: patient-specific finite element models to predict surgical outcomes. Computer Methods in Biomechanics and Biomedical Engineering 8, 259–265.

Melenk, J.M., Babuška, I., 1996. The partition of unity finite element method: basic theory and applications. Computer Methods in Applied Mechanics and Engineering 139, 289–314.

Nakaji, P., Spetzler, R., 2004. Innovations in surgical approach: the marriage of technique, technology, and judgment. Clinical neurosurgery 51, 177–185.

Neal, M.L., Kerckhoffs, R., 2010. Current progress in patient-specific modeling. Briefings in Bioinformatics 11, 111–126.

Oguro, S., Tuncali, K., Elhawary, H., Morrison, P.R., Hata, N., Silverman, S.G., 2011. Image registration of pre-procedural MRI and intra-procedural CT images to aid CT-guided percutaneous cryoablation of renal tumors. International Journal of Computer Assisted Radiology and Surgery 6, 111–117.

Picinbono, G., Delingette, H., Ayache, N., 2003. Non-linear anisotropic elasticity for real-time surgery simulation. Graphical Models 65, 305–321.

Warfield, S.K., Haker, S.J., Talos, I.F., Kemper, C.A., Weisenfeld, N., Mewes, A.U.J., Goldberg-Zimring, D., Zou, K.H., 2005. Capturing intraoperative deformations: research experience at Brigham and Women's Hospital. Medical Image Analysis 9, 145–162.

Wittek, A., Hawkins, T., Miller, K., 2009. On the unimportance of constitutive models in computing brain deformation for image-guided surgery. Biomechanics and Modeling in Mechanobiology 8, 77–84.

Wittek, A., Joldes, G., Couton, M., Warfield, S.K., Miller, K., 2010. Patient-specific non-linear finite element modelling for predicting soft organ deformation in real-time; Application to non-rigid neuroimage registration. Progress in biophysics and molecular biology 103, 292–303.

Wittek, A., Miller, K., Kikinis, R., Warfield, S.K., 2007. Patient-specific model of brain deformation: application to medical image registration. Journal of Biomechanics 40, 919–929.

Yang, K.H., King, A.I., 2011. Modeling of the brain for injury simulation and prevention. In: Miller, K. (Ed.), Biomechanics of the Brain. Springer, New York, pp. 91–110.